Epsilon-Tube Filtering: Reduction of High-Amplitude Motion Artifacts From Impedance Plethysmography Signal

Sardar Ansari, *Member, IEEE*, Kevin Ward, and Kayvan Najarian, *Senior Member, IEEE*

***Abstract*—The impedance plethysmography (IP) has long been used to monitor respiration. The IP signal is also suitable for portable monitoring of respiration due to its simplicity. However, this signal is very susceptible to motion artifact (MA). As a result, MA reduction is an indispensable part of portable acquisition of the IP signal. Often, the amplitude of the MA is much larger than the amplitude of the respiratory component in the IP signal. This study proposes a novel filtering method to remove the high-amplitude MA's from the IP signal. The proposed method combines the idea of ε-tube loss function and an autoregressive exogenous model to estimate the MA while leaving the periodic respiratory component of the IP signal intact. Also, a regularization method is used to find the best filter coefficients that maximize the regularity of the output signal. The results indicate that the proposed method can effectively remove the MA, outperforming the popular MA reduction methods. Several different performance measures are used for the comparison and the differences are found to be statistically significant.**

***Index Terms*—Autoregressive exogenous model, epsilon-tube, impedance plethysmography, motion artifact reduction, portable monitoring of respiration.**

I. Introduction

MOTION artifact (MA) reduction is one of the most challenging problems encountered during filtering and processing of physiological signals, especially those that are collected using portable monitoring devices. The main difficulty in dealing with MA is its dynamic nature and the fact that the amplitude of such artifacts is often much larger than the amplitude of the signal of interest. The previous studies that address this problem can be broadly divided into three groups. The first group is focused on instrumentation. The aim of these studies is to provide alternative instruments for signal recording, such as electrodes, sensors, or wires, as well as different electrode placements that are less susceptible to MA [1], [2]. Such improvements are outside the scope of this paper.

The second group uses independent component analysis (ICA) and principal component analysis (PCA) to estimate the MA as an independent source of variation in the signal [3]–[6]. The goal of ICA is to estimate the set of linear coefficients through which the signal of interest and the MA have been mixed. It requires multichannel recordings of the signal which are often available for the electrocardiogram (ECG) and electroencephalography signals. However, the IP signal is typically measured through a single channel recording. The multichannel recording of the IP signal will require excessive instrumentation and hardware which is not desirable when designing a portable device. Therefore, ICA is not an appropriate candidate for MA reduction from the IP signal here. Another disadvantage of using ICA is that the assumption of linear mixing process is not guaranteed to hold.

The third group of MA reduction methods uses adaptive filters to estimate the MA. Different varieties of adaptive filters have been applied to this problem including least mean squares (LMS) [7]–[9], recursive least squares (RLS), [10], [11], normalized LMS (NLMS) [12], and normalized signed regressor LMS [13]. Despite the popularity of adaptive filters, there is a disadvantage associated with them. Adaptive filters tend to not only model the MA, but they can also adapt to the signal of interest. In particular, the MA in the IP signal is similar in shape and frequency bandwidth to the respiratory component of the signal. Therefore, an adaptive filter that successfully models the MA will also model the respiratory component in the calm (not contaminated by MA) sections of the signal. This is due to the fact that adaptive filters do not have a mechanism to distinguish between the MA and the component of interest when they are similar. However, the ε-tube filtering method that is proposed in this paper focuses only on the MA and is not affected by the semisinusoidal pattern of the respiratory component of the IP signal.

The proposed filtering method is applied to the IP signal to eliminate the MA. The main component of this signal is highly correlated with respiration which has a regular periodic pattern with an amplitude that is almost constant within a short window of time. The amplitude of the interfering MA is often larger than the amplitude of the respiratory component. Therefore, the proposed filtering method can be applied to this signal to remove the MA. The end-tidal CO_2 ($EtCO_2$) signal is used as the reference signal in this study to compare the filter output to the actual respiration waveform. The $EtCO_2$ signal is considered the gold standard in monitoring the respiration. In order to show that

Manuscript received September 18, 2013; revised January 20, 2014; accepted March 31, 2014; Date of publication April 9, 2014; date of current version March 2, 2015. This work was supported by the U.S. Army Medical Research and Material Command Combat Casualty Care Research Program under Grant 05-0033-02. The opinions expressed herein are the personal opinions of the authors and are not to be construed as representing those of the Department of Defense, the Department of the Army, or the U.S. Army.

S. Ansari is with the Department of Computer Science and the Department of Statistical Sciences and Operations Research, Virginia Commonwealth University, Richmond, VA 23284 USA (e-mail: ansaris@vcu.edu).

K. Ward is with the Department of Emergency Medicine, University of Michigan, Ann Arbor, MI 48105 USA (e-mail: keward@med.umich.edu).

K. Najarian is with the Department of Computational Medicine and Bioinformatics, University of Michigan, Ann Arbor, MI 48109 USA (e-mail: kayvan@umich.edu).

Digital Object Identifier 10.1109/JBHI.2014.2316287

the ε-tube filtering, in fact, has a better performance compared to the currently existing methods, it is compared to the ICA algorithm, and the RLS and NLMS filtering methods in the results section.

The remainder of this paper is organized as follows. Next section will introduce the IP signal and the respiratory rate. Section III introduces the proposed filtering method. The regularization term is discussed in Section IV, and the gradients of the objective function and the constrains are derived in Section V. The nonrecursive version of the gradients for fast computing are presented in Section VI. Finally, Section IX discusses the conclusions and the future work.

II. Impedance Plethysmography and Respiratory Rate

Measuring electrical impedance of different segments of the body, a.k.a. IP, has been widely used in different fields of medicine for decades. Examples of applications of plethysmography in medicine are measuring lung volume, blood volume variations, blood flow, muscle contraction, eye movement, autonomic nervous system activity, and activity of brain cells [14].

Plethysmography is performed by injecting a high-frequency low-amplitude sinusoidal current into the segment of interest using a pair of skin electrodes (current electrodes) and measuring the imposed voltage difference between the injection points using another pair of skin electrodes (voltage electrodes) [15]. Electrical resistance of the tissue of interest is then calculated using the injected current and the measured voltage difference between the electrodes, which is caused by the passage of current through the tissue. The result is the IP signal, whose main component is highly correlated with respiration [16], [17]. The respiratory signal and the respiratory rate could be easily extracted from the IP signal acquired from the thorax and abdomen area when the subject is motionless. However, motion is another main source of blood volume variation. Motion can create drastic variations in the measured IP signal [18]–[22], resulting in artifacts whose amplitudes are much larger than the amplitude of the respiratory component in many cases [23]. As a result, it is necessary to use filtering methods to eliminate MA's before the signal can be used to monitor respiration. The IP signals used in this study are measured on the subject's back between the third and tenth ribs. This setting has been used instead of the traditional transthoracic electrode placement, since it is suitable for portable acquisition of the IP signal.

III. ε-Tube and Autoregressive Exogenous Models

The idea of using ε-tube along with the tangent sigmoid (TS) activation functions (AF) was first introduced in our previous paper [24]. However, the TS functions have a predetermined and rigid structure that prevents it from modeling complex MA's effectively. In particular, the derivative of the TS function does not change sign. Therefore, a new TS function is required every time the derivative of the MA changes sign. Instead, we use an autoregressive exogenous (ARX) model here in order to increase the flexibility of the model. The concept of ε-tube was first introduced in the context of support vector machines and support vector regression in the form of Vapnik's loss function [25]. Unlike the conventional Euclidean norms, Vapnik's loss function allows for a margin, called the tube, where the error that is assigned to the points that fall inside the tube is zero. In mathematical terms,

$$|g_t - y_t(\mathbf{U}, \mathbf{w})|_\varepsilon = \max(0, |g_t - y_t(\mathbf{U}, \mathbf{w})| - \varepsilon) \quad (1)$$

where g_t is the value of the signal at time t, y_t is the output of the filter at t, $\mathbf{U}$ is a matrix whose rows are the accelerometer signals, $\mathbf{w}$ is the vector of filter coefficients, and ε is the width of the tube. In other words, the points for which the distance between the model output and the target value is less than ε (points that fall within the tube) will be assigned a zero error. Moreover, the error increases in a linear fashion outside the tube. Therefore, the ε-tube filtering seems to be a natural fit for removing MA's with high amplitude from periodic signals. The assumptions made here are that the amplitude of the periodic signal does not change rapidly in a short period of time and that the signal has a regular recurring pattern. For example, the main component of the IP signal is respiration which is periodic with an almost constant amplitude within short windows of time. Therefore, ε-tube can be used to estimate the MA while it refrains from modeling the respiratory component of the signal by forming a tube around it that only encompasses the respiratory component.

The ε-tube filter is formulated as a constrained optimization problem which can be expressed as

$$\text{Minimize} \sum_{t=0}^{N-1} \zeta_t + \sum_{t=0}^{N-1} \zeta_t' \quad (2)$$

subject to

$$g_t - y_t(\mathbf{U}, \mathbf{w}) \le \varepsilon + \zeta_t, \quad t = 0, \ldots, N-1 \quad (3)$$

$$y_t(\mathbf{U}, \mathbf{w}) - g_t \le \varepsilon + \zeta_t', \quad t = 0, \ldots, N-1 \quad (4)$$

$$\zeta_t \ge 0, \quad \zeta_t' \ge 0, \quad t = 0, \ldots, N-1 \quad (5)$$

where ζ_t and ζ_t' are slack variables and N is the length of the signal.

In our previous work, $y_t(\mathbf{U}, \mathbf{w})$ was a combination of TS functions that modeled the MA. However, the TS functions are too rigid and are not flexible enough to model complex MA's. As a result, an ARX model is used in this paper enabling the filter to model MA's with generic shapes. The ARX model is defined as

$$y_t = -\sum_{i=1}^{n_a} a_i y_{t-i} + \sum_{i=1}^{n_b} \mathbf{b}_i^{\mathrm{T}} \mathbf{u}_{t-i+1} \quad (6)$$

where n_a, the number of poles, and n_b, the number of zeros plus 1, are design parameters. Also, a_i is the ith feedback coefficient, $\mathbf{u}_t$ is the vector of accelerometer readings at time t (the column of $\mathbf{U}$ associated with t), and $\mathbf{b}_i$ is the corresponding vector of the ith feedforward coefficients. Hence, the vector $\mathbf{w}$ in (1) is composed of a_i's and the elements of $\mathbf{b}_i$'s. Therefore, the problem reduces to finding the vector $\mathbf{w}$ that minimizes (2) subject to (3), (4), and (5). The solution to this optimization problem is unique only if the signal of interest is exactly periodic with a constant amplitude and a regular pattern, and the MA is

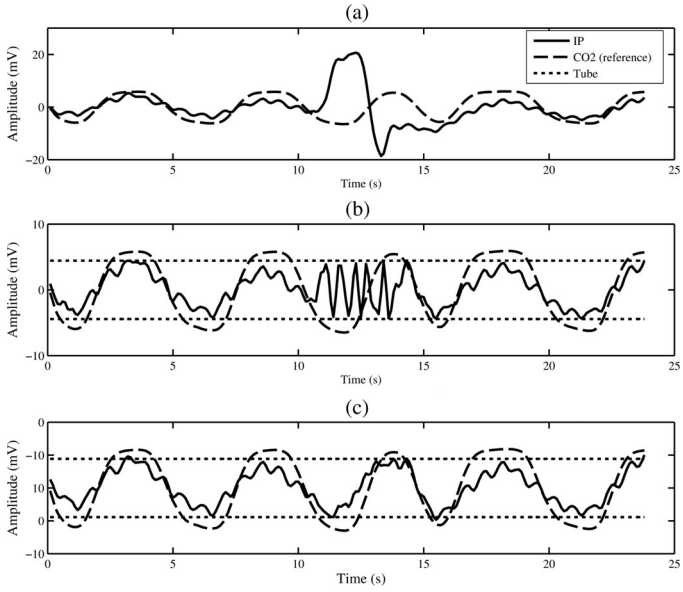

Fig. 1. (a) Instance of the IP signal contaminated by MA, (b) Filtered using ε-tube method without regularization, and (c) Filtered using ε-tube method with regularization. It is evident in (b) that the ε-tube by itself is not able to successfully remove the MA, although, the error is zero with respect to the ε-tube norm. On the other hand, using the regularization term in (3) leads to the successful removal of MA.

generated through an ARX process. However, none of these assumptions hold in reality; thus, the optimal solution is not unique. Instead, there is a set of filter coefficients all of which minimize the objective function in (2). This set includes the coefficients by which the MA has been generated. Fig. 1(a) shows an IP signal that is corrupted by MA. The same signal is shown in Fig. 1(b) after it was filtered using ε-tube as defined by (2)–(6). The filtered signal has an error of zero; thus, it is an optimal solution to the optimization problem. However, it does not resemble the shape of the respiratory component and contains some high-frequency noise. As a result, a second criterion is needed to choose the solution that is most likely to be the generator of the MA. Assuming that the IP signal follows a regular pattern, we use regularity of the signal as the second objective to maximize:

$$\text{Minimize } f = \sum_{t=0}^{N-1} \zeta_t + \sum_{t=0}^{N-1} \zeta_t' - cR(\mathbf{s}, \mathbf{U}, \mathbf{w}) \qquad (7)$$

where $R(\mathbf{s}, \mathbf{U}, \mathbf{w})$ is a regularization term, discussed in the next section, and c is a design parameter which adjusts the balance between the two objectives. The parameter c should be typically set to a small enough value so that the regularization term acts as a secondary objective, ensuring that we are searching for the solution with the most regular pattern among the ones that have the smallest error. The regularization term is discussed in the next section.

IV. Regularization

As discussed in the previous section, one needs to use a regularity measure to choose the ARX coefficients, among the ones that minimize the Vapnik norm, that lead to the most regular results. It is worth noting that the notion of regularity discussed here is different from the regularization in statistics and machine learning. Here, a regular signal is one that has a constant recurring pattern and regularity is the quantity which measures this characteristic. Consequently, a regular signal has a frequency composition that is invariant as time progresses. One way to measure this property is to use Stockwell transform (S-transform) [26]. S-transform is a generalization of short time Fourier transform and provides a time–frequency representation of the signal that is sensitive to irregularities in the signal. Fig. 2 shows an example of the magnitude of the S-transform of an IP signal that contains irregularities after it was filtered using the ε-tube without regularization. An ideal signal with a regular pattern would have a S-transform for which the frequency decompositions along the frequency axis for any two given points on the time axis are identical. Hence, the average correlation between the vertical slices of the S-transform in Fig. 2 can be used as a measure for the regularity of the signal. It is noteworthy that several other regularization terms were investigated in this study, e.g., several measures were extracted from the Fourier transform of the signal, including variance, kurtosis, and entropy, as well as several features extracted from the Wavelet transformation of the signal. However, S-transform proved to be the most sensitive to the irregularities in the signal. Therefore, it has been used in this study.

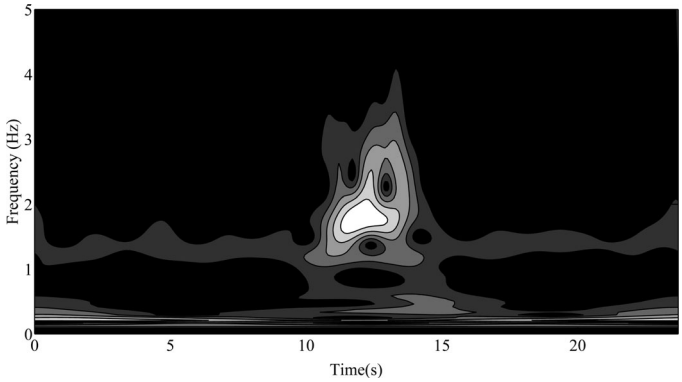

Fig. 2. S-transform of an irregular signal. The S-transform reflects the irregularities as high magnitude components around $t = 12$ s and $f = 2$ Hz.

The discrete S-transform of $y[kT]$ is a linear transformation defined as

$$\mathcal{S}_y\left[pT, \frac{n}{NT}\right] = \sum_{m=0}^{N-1} Y\left[\frac{m+n}{NT}\right] e^{-\frac{2\pi^2 m^2}{n^2}} e^{\frac{j2\pi mp}{N}}, \quad n \neq 0 \qquad (8)$$

and

$$\mathcal{S}_y\left[pT, \frac{n}{NT}\right] = \frac{1}{N}\sum_{m=0}^{N-1} y\left[\frac{m}{NT}\right], \quad n = 0 \qquad (9)$$

where Y is the Fourier transform of y; p and n are the time and frequency indices of the S-transform, respectively, N is the number of samples in the signal, and T is the sampling interval.

Also, the inverse S-transform of $\mathcal{S}_y$ is defined as

$$y[kT] = \frac{1}{N}\sum_{n=0}^{N-1}\sum_{p=0}^{N-1}\mathcal{S}_y\left[pT, \frac{n}{NT}\right]e^{\frac{j2\pi nk}{N}}. \tag{10}$$

In the rest of this paper, $\mathcal{S}_y[pT, \frac{n}{NT}]$ is denoted by $\mathcal{S}_y^{p,n}$. Stockwell [27] proposes a Shift theorem for the continuous S-transform. Here, we present similar results for the discrete case.

Theorem 1: The Shift theorem for the discrete S-transform: Assume that the S-transform of $y[kT]$ is $\mathcal{S}_y^{p,n}$, i.e.,

$$y[kT] \overset{\mathcal{S}}{\longleftrightarrow} \mathcal{S}_y^{p,n}. \tag{11}$$

Then, the S-transform of y after being translated by r samples can be calculated as

$$y[(k-r)T] \overset{\mathcal{S}}{\longleftrightarrow} e^{\frac{-j2\pi nr}{N}}\mathcal{S}_y^{p-r,n}. \tag{12}$$

The proof can be found in Appendix. A negative shift will represent a circular shift toward the older signal values in the rest of this paper.

The S-transform of (6), denoted by $\mathcal{S}_y$, can be obtained using Theorem 1 as

$$\begin{aligned}\mathcal{S}_y^{p,n} &= \mathcal{S}\left\{-\sum_{i=1}^{n_a}a_i y_{t-i} + \sum_{i=1}^{n_b}\mathbf{b}_i^{\mathrm{T}}\mathbf{u}_{t-i+1}\right\}\\ &= -\sum_{i=1}^{n_a}a_i\mathcal{S}\{y_{t-i}\} + \sum_{i=1}^{n_b}\mathbf{b}_i^{\mathrm{T}}\mathcal{S}\{\mathbf{u}_{t-i+1}\}\\ &= -\sum_{i=1}^{n_a}a_i e^{\frac{-j2\pi ni}{N}}\mathcal{S}_y^{p-i,n} + \sum_{i=1}^{n_b}\mathbf{b}_i^{\mathrm{T}}e^{\frac{-j2\pi n(i-1)}{N}}\mathcal{S}_{\mathbf{u}}^{p-i+1,n}\end{aligned} \tag{13}$$

where $\mathcal{S}\{\mathbf{u}_{t-i+1}\}$ indicates applying S-transform to the rows of $\mathbf{U}$ (accelerometer signals) after they were shifted by $i-1$ samples and $\mathcal{S}_{\mathbf{u}}^{p-i+1,n}$ is a column vector whose hth element is the S-transform of the hth row of $\mathbf{U}$ at $p-i+1$ and n.

Finally, we define the regularization term as

$$R(\mathbf{s}, \mathbf{u}_t, \mathbf{w}) = \frac{1}{N^2}\sum_p\sum_q \log(|r_{pq}|) \tag{14}$$

where r_{pq} is the Pearson correlation coefficient between $\mathcal{S}_{g-y}^{p,n}$ and $\mathcal{S}_{g-y}^{q,n}$. Note that we use $\log(|\cdot|)$ in (14) since the natural log of the magnitude of a complex number is differentiable. The results of filtering the IP signal in Fig. 1(a) using the ε-tube method and the regularization term in (14) are shown in Fig. 1(c). The proposed filtering method is successful in removing the MA and recovering the respiratory component of the signal. Regularization leads the optimization process toward the right filter coefficients and successfully removes the irregularities in the signal. The S-transform of the filtered signal is free of the high-frequency noise that was present in Fig. 2. The vertical slices of the S-transform (the frequency components at different times) are correlated. The low-amplitude variations on top of the IP signal that correspond to the heart rate are deteriorated after filtering in Fig. 1(c). The discontinuity in the horizontal band at $f = 1.3$ Hz in Fig. 3 is caused by this deterioration. However, the goal of this filter is to maintain the respiratory component of the signal and not the heart rate. All in all, the proposed filter is able to successfully recover the IP signal that is contaminated by MA.

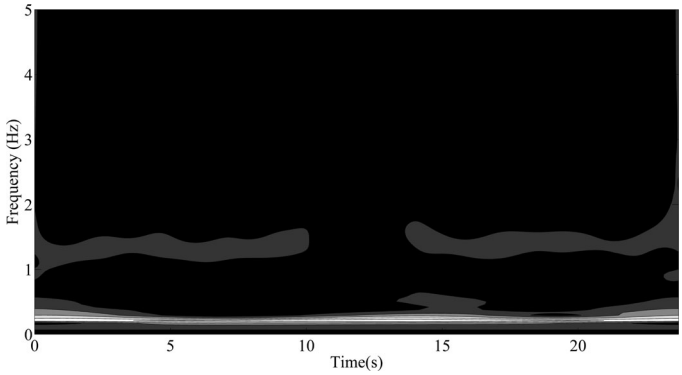

Fig. 3. S-transform of a regular signal (after MA removal). The decomposition has an almost constant frequency pattern along the time axis. The white band around $f = 0.25$ Hz corresponds to respiration which is the dominant component of the signal. The gray band around $f = 1.3$ Hz corresponds to heart rate that is the second most dominant component of the signal.

In order to find the optimal solution to (7) subject to (3)–(5), one needs to compute the gradients of the objective function and the constraints. These gradients are computed in the next section.

V. Gradients

The gradients of (3)–(5) and (7) are found in this section. We start with finding recursive formulas for the partial derivatives of y_t.

$$\begin{aligned}\frac{\partial}{\partial a_l}y_t &= \frac{\partial}{\partial a_l}\left(-\sum_{i=1}^{n_a}a_i y_{t-i} + \sum_{i=1}^{n_b}\mathbf{b}_i^{\mathrm{T}}\mathbf{u}_{t-i+1}\right)\\ &= -\sum_{i=1}^{n_a}a_i\frac{\partial}{\partial a_l}y_{t-i} - y_{t-l},\end{aligned} \tag{15}$$

for $t = 0, \ldots, N-1$ and $l = 1, \ldots, n_a$. Also,

$$\begin{aligned}\frac{\partial}{\partial b_l^h}y_t &= \frac{\partial}{\partial b_l^h}\left(-\sum_{i=1}^{n_a}a_i y_{t-i} + \sum_{i=1}^{n_b}\mathbf{b}_i^{\mathrm{T}}\mathbf{u}_{t-i+1}\right)\\ &= -\sum_{i=1}^{n_a}a_i\frac{\partial}{\partial b_l^h}y_{t-i} + u_{t-l+1}^h\end{aligned} \tag{16}$$

where u_{t-l+1}^h is the hth element in vector $\mathbf{u}_{t-i+1}$, i.e., the reading for the hth input accelerometer signal at time $t-l+1$, for $t = 0, \ldots, N-1$ and $l = 1, \ldots, n_b$. Therefore, the partial derivatives of (3) and (4) with regards to a_l and b_l can be recursively calculated using (15) and (16). Moreover, the partial derivatives of (3) with respect to ζ_t and ζ_t' are -1 and 0, respectively. Likewise, the partial derivatives of (4) is 0 with respect to ζ_t and -1 with respect to ζ_t'. The partial derivatives of (5) are trivial.

Next, we compute the gradient of $\mathcal{S}_y^{p,n}$ which is composed of the partial derivatives with respect to a_l and b_l. It will be used later to derive the gradient of (7). The partial derivative of

S-transform with respect to a_l can be found as

$$\begin{aligned}\frac{\partial}{\partial a_l}\mathcal{S}_y^{p,n} &= \mathcal{S}\left\{-\sum_{i=1}^{n_a} a_i \frac{\partial}{\partial a_l} y_{t-i} - y_{t-l}\right\} \\ &= -\sum_{i=1}^{n_a} a_i \frac{\partial}{\partial a_l}\mathcal{S}\{y_{t-i}\} - \mathcal{S}\{y_{t-l}\} \\ &= -\sum_{i=1}^{n_a} a_i \frac{\partial}{\partial a_l}\left(e^{\frac{-j2\pi ni}{N}}\mathcal{S}_y^{p-i,n}\right) - e^{\frac{-j2\pi nl}{N}}\mathcal{S}_y^{p-l,n} \\ &= -\sum_{i=1}^{n_a} a_i e^{\frac{-j2\pi ni}{N}}\frac{\partial}{\partial a_l}\mathcal{S}_y^{p-i,n} - e^{\frac{-j2\pi nl}{N}}\mathcal{S}_y^{p-l,n}.\end{aligned} \tag{17}$$

Similarly, the partial derivative of $\mathcal{S}_y^{p,n}$ with respect to b_l^h is

$$\begin{aligned}\frac{\partial}{\partial b_l^h}\mathcal{S}_y^{p,n} &= \mathcal{S}\left\{-\sum_{i=1}^{n_a} a_i \frac{\partial}{\partial b_l^h} y_{t-i} + u_{t-l+1}^h\right\} \\ &= -\sum_{i=1}^{n_a} a_i \frac{\partial}{\partial b_l^h}\mathcal{S}\{y_{t-i}\} + \mathcal{S}\left\{u_{t-l+1}^h\right\} \\ &= -\sum_{i=1}^{n_a} a_i \frac{\partial}{\partial b_l^h}\left(e^{\frac{-j2\pi ni}{N}}\mathcal{S}_y^{p-i,n}\right) + e^{\frac{-j2\pi n(l-1)}{N}}\mathcal{S}_{u^h}^{p-l+1,n} \\ &= -\sum_{i=1}^{n_a} a_i e^{\frac{-j2\pi ni}{N}}\frac{\partial}{\partial b_l^h}\mathcal{S}_y^{p-i,n} + e^{\frac{-j2\pi n(l-1)}{N}}\mathcal{S}_{u^h}^{p-l+1,n}\end{aligned} \tag{18}$$

where $\mathcal{S}_{u^h}^{p-l+1,n}$ is the S-transform of the hth row of $\mathbf{U}$ at $p-l+1$ and n. Equations (17) and (18) can be used to recursively compute the gradient of the S-transform.

The partial derivative of the objective function, (7), with respect to a_l can be obtained as

$$\begin{aligned}\frac{\partial}{\partial a_l} f &= \frac{\partial}{\partial a_l}\left(\sum_{t=0}^{N-1}\zeta_t + \sum_{t=0}^{N-1}\zeta_t' - cR(\mathbf{s},\mathbf{U},\mathbf{w})\right) \\ &= -c\frac{\partial}{\partial a_l}R(\mathbf{s},\mathbf{U},\mathbf{w}) \\ &= -\frac{c}{N^2}\sum_p\sum_q \frac{\partial}{\partial a_l}\log(|r_{pq}|).\end{aligned} \tag{19}$$

It is shown in [28] that the log of a complex number can be written as

$$\log(r_{pq}) = \log(|r_{pq}|) + j(\arg(r_{pq}) + 2\pi k) \tag{20}$$

for integer k's. Therefore, the derivative of $\log(|r_{pq}|)$ can be found as

$$\frac{\partial}{\partial a_l}\log(|r_{pq}|) = \mathrm{Re}\left[\frac{\partial}{\partial a_l}\log(r_{pq})\right] \tag{21}$$

where $\mathrm{Re}[.]$ denotes the real part of a complex number. Therefore,

$$\frac{\partial}{\partial a_l} f = -\frac{c}{N^2}\sum_p\sum_q \mathrm{Re}\left[\frac{\partial}{\partial a_l}\log(r_{pq})\right]. \tag{22}$$

The Pearson correlation coefficient between $\mathcal{S}_{g-y}^{p,n}$ and $\mathcal{S}_{g-y}^{q,n}$ is defined as

$$r_{pq} = \frac{s_{pq}}{\sqrt{s_{pp}s_{qq}}} \tag{23}$$

where s_{pq} is the covariance between $\mathcal{S}_{g-y}^{p,n}$ and $\mathcal{S}_{g-y}^{q,n}$ and s_{pp} is the variance of $\mathcal{S}_{g-y}^{p,n}$. Thus,

$$\log(r_{pq}) = \log(s_{pq}) - \frac{1}{2}\log(s_{pp}) - \frac{1}{2}\log(s_{qq}) \tag{24}$$

and

$$\frac{\partial}{\partial a_l}\log(r_{pq}) = \frac{\partial s_{pq}/\partial a_l}{s_{pq}} - \frac{1}{2}\frac{\partial s_{pp}/\partial a_l}{s_{pp}} - \frac{1}{2}\frac{\partial s_{qq}/\partial a_l}{s_{qq}}. \tag{25}$$

The covariance of $\mathcal{S}_{g-y}^{p,n}$ and $\mathcal{S}_{g-y}^{q,n}$ is defined as

$$s_{pq} = \frac{1}{N-1}\left(\sum_{n=1}^{N}\overline{\mathcal{S}_{g-y}^{p,n}}\mathcal{S}_{g-y}^{q,n} - \frac{1}{N}\left(\sum_{n=1}^{N}\overline{\mathcal{S}_{g-y}^{p,n}}\right)\left(\sum_{n=1}^{N}\mathcal{S}_{g-y}^{q,n}\right)\right) \tag{26}$$

where $\overline{\mathcal{S}_{g-y}^{p,n}}$ is the complex conjugate of $\mathcal{S}_{g-y}^{p,n}$. Consequently, the derivative of s_{pq} with respect to a_l can be computed as following:

$$\begin{aligned}\frac{\partial}{\partial a_l}s_{pq} = \frac{1}{N-1}\Bigg[&\sum_{n=1}^{N}\left(\frac{\partial}{\partial a_l}\overline{\mathcal{S}_{g-y}^{p,n}}\mathcal{S}_{g-y}^{q,n} + \overline{\mathcal{S}_{g-y}^{p,n}}\frac{\partial}{\partial a_l}\mathcal{S}_{g-y}^{q,n}\right) \\ &- \frac{1}{N}\left(\sum_{n=1}^{N}\frac{\partial}{\partial a_l}\overline{\mathcal{S}_{g-y}^{p,n}}\right)\left(\sum_{n=1}^{N}\mathcal{S}_{g-y}^{q,n}\right) \\ &- \frac{1}{N}\left(\sum_{n=1}^{N}\overline{\mathcal{S}_{g-y}^{p,n}}\right)\left(\sum_{n=1}^{N}\frac{\partial}{\partial a_l}\mathcal{S}_{g-y}^{q,n}\right)\Bigg].\end{aligned} \tag{27}$$

By rearranging, we obtain

$$\begin{aligned}\frac{\partial}{\partial a_l}s_{pq} = &\frac{1}{N-1}\Bigg[\sum_{n=1}^{N}\frac{\partial}{\partial a_l}\overline{\mathcal{S}_{g-y}^{p,n}}\mathcal{S}_{g-y}^{q,n} \\ &- \frac{1}{N}\left(\sum_{n=1}^{N}\frac{\partial}{\partial a_l}\overline{\mathcal{S}_{g-y}^{p,n}}\right)\left(\sum_{n=1}^{N}\mathcal{S}_{g-y}^{q,n}\right)\Bigg] \\ &+ \frac{1}{N-1}\Bigg[\sum_{n=1}^{N}\overline{\mathcal{S}_{g-y}^{p,n}}\frac{\partial}{\partial a_l}\mathcal{S}_{g-y}^{q,n} \\ &- \frac{1}{N}\left(\sum_{n=1}^{N}\overline{\mathcal{S}_{g-y}^{p,n}}\right)\left(\sum_{n=1}^{N}\frac{\partial}{\partial a_l}\mathcal{S}_{g-y}^{q,n}\right)\Bigg] \\ = &\, s_{p(l)q} + s_{pq(l)}\end{aligned} \tag{28}$$

where $s_{p(l)q}$ denotes the covariance between $\frac{\partial}{\partial a_l}\mathcal{S}_{g-y}^{p,n}$ and $\mathcal{S}_{g-y}^{q,n}$, and $s_{pq(l)}$ denotes the covariance between $\mathcal{S}_{g-y}^{p,n}$ and $\frac{\partial}{\partial a_l}\mathcal{S}_{g-y}^{q,n}$.

Also, it is easy to show that

$$\frac{\partial}{\partial a_l} s_{pp} = 2s_{p(l)p}, \quad \frac{\partial}{\partial a_l} s_{qq} = 2s_{qq(l)}. \tag{29}$$

Substituting (28) and (29) into (25), one finds

$$\frac{\partial}{\partial a_l} \log(r_{pq}) = \frac{s_{p(l)q} + s_{pq(l)}}{s_{pq}} - \frac{s_{p(l)p}}{s_{pp}} - \frac{s_{qq(l)}}{s_{qq}}. \tag{30}$$

Hence, the derivative of the objective function with respect to a_l is

$$\begin{aligned}\frac{\partial}{\partial a_l} f &= -\frac{c}{N^2} \sum_p \sum_q \mathrm{Re}\left(\frac{s_{p(l)q} + s_{pq(l)}}{s_{pq}} - \frac{s_{p(l)p}}{s_{pp}} - \frac{s_{qq(l)}}{s_{qq}}\right) \\ &= -\frac{2c}{N^2} \sum_p \sum_q \mathrm{Re}\left(\frac{s_{p(l)q}}{s_{pq}}\right) + \frac{2c}{N} \sum_p \mathrm{Re}\left(\frac{s_{p(l)p}}{s_{pp}}\right).\end{aligned} \tag{31}$$

The derivative of f with respect to b_l^h can be computed in a similar manner

$$\frac{\partial}{\partial b_l^h} f = -\frac{2c}{N^2} \sum_p \sum_q \mathrm{Re}\left(\frac{s_{p(l,h)q}}{s_{pq}}\right) + \frac{2c}{N} \sum_p \mathrm{Re}\left(\frac{s_{p(l,h)p}}{s_{pp}}\right) \tag{32}$$

where $s_{p(l,h)q}$ denotes the covariance between $\frac{\partial}{\partial b_l^h}\mathcal{S}_{g-y}^{p,n}$ and $\mathcal{S}_{g-y}^{q,n}$. The partial derivatives of f with respect to ζ_t and ζ_t' are equal to 1. Therefore, we obtained the gradient of f by deriving all of its partial derivatives.

The recursive equations introduced in this section are suitable for real-time filtering of the IP signal. There are cases when the process takes place in batch mode. Recursive equations will be very inefficient in such applications. Hence, nonrecursive versions of the same equations are derived in the next section for batch processing.

VI. Implementation

Previous section introduced recursive equations to compute y_t, $\frac{\partial}{\partial a_l} y_t$, $\frac{\partial}{\partial b_l^h} y_t$, $S_y^{p,n}$, $\frac{\partial}{\partial a_l} S_y^{p,n}$, and $\frac{\partial}{\partial b_l^h} S_y^{p,n}$. Recursive equations are desirable in adaptive filters. However, evaluating these equations is inefficient in nonadaptive settings. Therefore, nonrecursive versions of the same equations are introduced in this section. The new equations, which are based on Fourier transform and inverse Fourier transform, can be evaluated more efficiently. The input signals are assumed to be circular, i.e., $y_{t+kN} = y_t$ for integer k's.

Let us define the matrix $\mathbf{C}$ and vectors $\mathbf{y}$ and $\mathbf{d}$ as follows:

$$\mathbf{C} = \begin{pmatrix} 1 & 0 & 0 & \cdots & 0 & a_{n_a} & a_{n_a-1} & \cdots & a_2 & a_1 \\ a_1 & 1 & 0 & \cdots & 0 & 0 & a_{n_a} & \cdots & a_3 & a_2 \\ a_2 & a_1 & 1 & \cdots & 0 & 0 & 0 & \cdots & a_4 & a_3 \\ \vdots & \vdots & \vdots & & \vdots & \vdots & \vdots & & \vdots & \vdots \\ 0 & 0 & 0 & \cdots & a_{n_a} & a_{n_a-1} & a_{n_a-2} & \cdots & a_1 & 1 \end{pmatrix} \tag{33}$$

$$\mathbf{y} = \begin{pmatrix} y_0 \\ y_1 \\ y_2 \\ \vdots \\ y_{N-1} \end{pmatrix}, \quad \mathbf{d} = \begin{pmatrix} d_0 \\ d_1 \\ d_2 \\ \vdots \\ d_{N-1} \end{pmatrix} \tag{34}$$

where $d_t = \sum_{i=1}^{n_b} \mathbf{b}_i^{\mathrm{T}} \mathbf{u}_{t-i+1}$. Thus, (6) can be expressed as

$$\mathbf{C}\mathbf{y} = \mathbf{d}. \tag{35}$$

Each row of the matrix $\mathbf{C}$ can be obtained by rotating the previous row by one element to the right. Therefore, $\mathbf{C}$ is a circulant matrix. As a result, (35) can be expressed as a convolution between the first column of $\mathbf{C}$, denoted by $\mathbf{c}$ and $\mathbf{y}$,

$$\mathbf{c} * \mathbf{y} = \mathbf{d}. \tag{36}$$

Applying Fourier transform to both sides, we obtain

$$\mathcal{F}\{\mathbf{c} * \mathbf{y}\} = \mathcal{F}\{\mathbf{d}\} \Rightarrow \mathcal{F}\{\mathbf{c}\} \cdot \mathcal{F}\{\mathbf{y}\} = \mathcal{F}\{\mathbf{d}\}. \tag{37}$$

Hence,

$$y_t = \mathcal{F}^{-1}\left\{\frac{\mathcal{F}\{\mathbf{d}\}_w}{\mathcal{F}\{\mathbf{c}\}_w}\right\}_t = \mathcal{F}^{-1}\left\{\frac{\hat{d}_w}{\hat{c}_w}\right\}_t. \tag{38}$$

Note that the division is element-wise. The vector $\mathbf{c}$ is treated as a signal when the Fourier transform is being computed. This signal can be expressed as

$$\mathbf{c}(i) = \delta(i) + a_1\delta(i-1) + a_2\delta(i-2) + \cdots + a_{n_a}\delta(i-n_a) \tag{39}$$

where $\delta(\cdot)$ denotes the Dirac delta function. The index i corresponds to the row number in vector $\mathbf{c}$. Also, it is the time index when $\mathbf{c}$ is treated as a signal. The two representations of $\mathbf{c}$, as a column vector and as a signal, are mathematically equivalent. The Fourier transform of $\mathbf{c}$ can be written as

$$\hat{c}_w = 1 + \sum_{i=1}^{n_a} a_i e^{\frac{-j2\pi iw}{N}} \tag{40}$$

by applying the Fourier transform to both sides of (39). Moreover, the Fourier transform of $\mathbf{d}$ can be found as

$$\hat{d}_w = \mathcal{F}\left\{\sum_{i=1}^{n_b} \mathbf{b}_i^{\mathrm{T}} \mathbf{u}_{t-i+1}\right\}_w = \sum_{i=1}^{n_b} \mathbf{b}_i^{\mathrm{T}} \{\hat{\mathbf{u}}_{-i+1}\}_w \tag{41}$$

where $\{\hat{\mathbf{u}}_{-i+1}\}_w$ is a vector whose hth element is computed by shifting u_t^h by $-i+1$ elements in a circular manner and then applying the Fourier transform to the shifted signal, evaluated at w. Substituting (40) and (41) into (38), we obtain

$$y_t = \mathcal{F}^{-1}\left\{\frac{\sum_{i=1}^{n_b} \mathbf{b}_i^{\mathrm{T}} \{\hat{\mathbf{u}}_{-i+1}\}_w}{1 + \sum_{i=1}^{n_a} a_i e^{\frac{-j2\pi iw}{N}}}\right\}_t. \tag{42}$$

Matrix $\mathbf{U}$ is composed of the input signals; hence, $\{\hat{\mathbf{u}}_{-i+1}\}_w$ can be computed prior to the optimization and be treated as constant thereafter. The term $e^{\frac{-j2\pi iw}{N}}$ can also be precomputed since they do not depend on the optimization variables. Therefore, the numerator and denominator in (42) are linear combinations of the optimization variables a_i and b_i^h. Computing y_t using (42) involves dividing two linear combinations and finding the

inverse Fourier transform of the result. Fourier transform of a signal and its inverse can be found very efficiently using the fast Fourier transform algorithm. On the other hand, using (6) to compute y_t involves an iterative procedure which can be very inefficient. The empirical observations indicate that computing y_t using (42) is on average 12.6 times faster than using (6).

The derivative of y_t with respect to a_l can be found in a similar manner. The recursive equation for $\frac{\partial}{\partial a_l} y_t$, (15), can be written as

$$\mathbf{C}\frac{\partial}{\partial a_l}\mathbf{y} = -\mathbf{y}_{-l} \tag{43}$$

where $\frac{\partial}{\partial a_l}\mathbf{y}$ is a vector composed of the derivatives of y_t with respect to a_l, and $\mathbf{y}_{-l}$ is the vector of y values after a shift of size $-l$, namely, y_{t-l}. Therefore, $\frac{\partial}{\partial a_l}\mathbf{y}$ can be found by taking the same steps as in (35)–(38), as follows:

$$\begin{aligned}\frac{\partial}{\partial a_l} y_t &= -\mathcal{F}^{-1}\left\{\frac{\mathcal{F}\{\mathbf{y}_{-l}\}_w}{\mathcal{F}\{\mathbf{c}\}_w}\right\}_t = -\mathcal{F}^{-1}\left\{\frac{\hat{y}_w e^{\frac{-j2\pi lw}{N}}}{\hat{c}_w}\right\}_t \\ &= -\mathcal{F}^{-1}\left\{\frac{\hat{y}_w}{1+\sum_{i=1}^{n_a} a_i e^{\frac{-j2\pi iw}{N}}}\right\}_{t-l}. \end{aligned}\tag{44}$$

Substituting the Fourier transform of the right-hand side of (42) for $\hat{y}_w$ yields

$$\frac{\partial}{\partial a_l} y_t = -\mathcal{F}^{-1}\left\{\frac{\sum_{i=1}^{n_b}\mathbf{b}_i^{\mathrm{T}}\{\hat{\mathbf{u}}_{-i+1}\}_w}{(1+\sum_{i=1}^{n_a} a_i e^{\frac{-j2\pi iw}{N}})^2}\right\}_{t-l}. \tag{45}$$

Furthermore, we can rewrite (16) as

$$\mathbf{C}\frac{\partial}{\partial b_l^h}\mathbf{y} = (\mathbf{u}_{-l+1}^h)^{\mathrm{T}} \tag{46}$$

where $\mathbf{u}_{-l+1}^h$ is the hth row of $\mathbf{U}$ after it is shifted by $-l+1$ elements. Therefore, the derivative of y_t with respect to b_l^h can be computed as

$$\frac{\partial}{\partial b_l^h} y_t = \mathcal{F}^{-1}\left\{\frac{\{\hat{\mathbf{u}}_{-l+1}^h\}_w^T}{1+\sum_{i=1}^{n_a} a_i e^{\frac{-j2\pi iw}{N}}}\right\}_t. \tag{47}$$

Next, we derive nonrecursive equations to compute $S_y^{p,n}$, $\frac{\partial}{\partial a_l} S_y^{p,n}$, and $\frac{\partial}{\partial b_l^h} S_y^{p,n}$. Let

$$\boldsymbol{\Lambda}^n = \begin{pmatrix} 1 & 0 & 0 & \cdots & 0 & \lambda_{n_a}^n & \lambda_{n_a-1}^n & \cdots & \lambda_2^n & \lambda_1^n \\ \lambda_1^n & 1 & 0 & \cdots & 0 & 0 & \lambda_{n_a}^n & \cdots & \lambda_3^n & \lambda_2^n \\ \lambda_2^n & \lambda_1^n & 1 & \cdots & 0 & 0 & 0 & \cdots & \lambda_4^n & \lambda_3^n \\ \vdots & \vdots & \vdots & & \vdots & \vdots & \vdots & & \vdots & \vdots \\ 0 & 0 & 0 & \cdots & \lambda_{n_a}^n & \lambda_{n_a-1}^n & \lambda_{n_a-2}^n & \cdots & \lambda_1^n & 1 \end{pmatrix} \tag{48}$$

and

$$\gamma_y^n = \begin{pmatrix} \mathcal{S}_y^{0,n} \\ \mathcal{S}_y^{1,n} \\ \mathcal{S}_y^{2,n} \\ \vdots \\ \mathcal{S}_y^{N-1,n} \end{pmatrix}, \quad \beta^{\mathbf{n}} = \begin{pmatrix} \beta_0^n \\ \beta_1^n \\ \beta_2^n \\ \vdots \\ \beta_{N-1}^n \end{pmatrix} \tag{49}$$

where $\lambda_i^n = a_i e^{\frac{-j2\pi ni}{N}}$ and $\beta_p^n = \sum_{i=1}^{n_b} \mathbf{b}_i^{\mathrm{T}} \mathcal{S}_{\mathbf{u}}^{p-i+1,n} e^{\frac{-j2\pi n(i-1)}{N}}$. Then, we can rewrite (13) using (48) and (49) as

$$\boldsymbol{\Lambda}^n \gamma_y^n = \boldsymbol{\beta}^n \tag{50}$$

which leads to

$$\mathcal{S}_y^{p,n} = \mathcal{F}^{-1}\left\{\frac{\hat{\beta}_w^n}{\hat{\lambda}_w^n}\right\}_p. \tag{51}$$

The first column of $\boldsymbol{\Lambda}^n$, when treated as a signal, can be expressed as

$$\begin{aligned}\lambda^n(i) = \delta(i) &+ a_1 e^{\frac{-j2\pi n}{N}}\delta(i-1) + a_2 e^{\frac{-j2\pi 2n}{N}}\delta(i-2) \\ &+ \cdots + a_{n_a} e^{\frac{-j2\pi n_a n}{N}}\delta(i-n_a)\end{aligned}\tag{52}$$

which has a Fourier transform of the form

$$\hat{\lambda}_w^n = 1 + \sum_{i=1}^{n_a} a_i e^{\frac{-j2\pi i(n+w)}{N}}. \tag{53}$$

Also, the Fourier transform of $\boldsymbol{\beta}^n$ can be derived as

$$\hat{\beta}_w^n = \sum_{i=1}^{n_b} \mathbf{b_i}^{\mathrm{T}} \left\{\hat{\mathcal{S}}_{\mathbf{u}}^{-i+1,n}\right\}_w e^{\frac{-j2\pi n(i-1)}{N}} \tag{54}$$

where $\mathcal{S}_{\mathbf{u}}^{-i+1,n}$ is a matrix whose hth row is the S-transform of the hth row of $\mathbf{u}$ at n after a shift of size $-i+1$, and $\{\hat{\mathcal{S}}_{\mathbf{u}}^{-i+1,n}\}_w$ is a vector whose hth element is the Fourier transform of the hth row of $\mathcal{S}_{\mathbf{u}}^{-i+1,n}$ evaluated at w. One can derive

$$\mathcal{S}_y^{p,n} = \mathcal{F}^{-1}\left\{\frac{\sum_{i=1}^{n_b} \mathbf{b_i}^{\mathrm{T}} \left\{\hat{\mathcal{S}}_{\mathbf{u}}^{-i+1,n}\right\}_w e^{\frac{-j2\pi n(i-1)}{N}}}{1+\sum_{i=1}^{n_a} a_i e^{\frac{-j2\pi i(n+w)}{N}}}\right\}_p \tag{55}$$

by substituting (53) and (54) into (51). Likewise, the similar equations for $\frac{\partial}{\partial a_l}\mathcal{S}_y^{p,n}$ and $\frac{\partial}{\partial b_l^h}\mathcal{S}_y^{p,n}$ can be written as

$$\frac{\partial}{\partial a_l}\mathcal{S}_y^{p,n} = -\mathcal{F}^{-1}\left\{\frac{\sum_{i=1}^{n_b} \mathbf{b_i}^{\mathrm{T}} \left\{\hat{\mathcal{S}}_{\mathbf{u}}^{-i+1,n}\right\}_w e^{\frac{-j2\pi n(l+i-1)}{N}}}{(1+\sum_{i=1}^{n_a} a_i e^{\frac{-j2\pi i(n+w)}{N}})^2}\right\}_{p-l} \tag{56}$$

$$\frac{\partial}{\partial b_l^h}\mathcal{S}_y^{p,n} = \mathcal{F}^{-1}\left\{\frac{\left\{\hat{\mathcal{S}}_{u^h}^{-i+1,n}\right\}_w}{1+\sum_{i=1}^{n_a} a_i e^{\frac{-j2\pi i(n+w)}{N}}}\right\}_p \tag{57}$$

where $\{\hat{\mathcal{S}}_{u^h}^{-i+1,n}\}_w$ is the hth element of $\{\hat{\mathcal{S}}_{\mathbf{u}}^{-i+1,n}\}_w$.

All of the derived nonrecursive equations involve linear combinations of the filter coefficients, vector and matrix multiplications, element-wise multiplications and divisions, and inverse Fourier transform. Modern computers can efficiently perform all of these operations. On the other hand, the recursive equations derived in the previous section are much more time consuming. In particular, the iterative equations can only be executed sequentially while the operations that are involved in the nonrecursive equations can be computed in parallel mode. Depending on the framework and application, one might choose to either use the recursive equations or the nonrecursive ones.

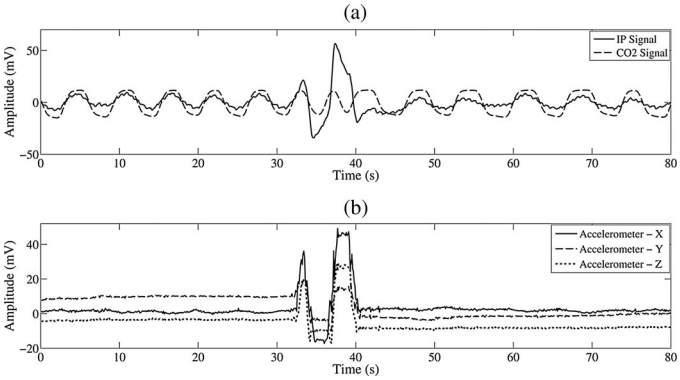

Fig. 4. Sample of the input signals contaminated by a movement that imitates opening a window. The IP and $EtCO_2$ signals are shown in (a) and (b) illustrates the accelerometer signals in *X*-, *Y*-, and *Z*-directions.

Fig. 5. Placements of electrodes.

VII. Experiments and Data

The experiments that are presented in this study were conducted using a Biopac MP150 system, equipped with a Biopac EBI100C to measure the IP signal and a Biopac CO2100C to measure the $EtCO_2$ signal. All the signals were collected at 250 Hz and were later down-sampled to 10 Hz for processing purposes. The collected IP signals were filtered using a Butterworth bandpass filter with cutoff frequencies of 0.001 and 2 Hz. A three-axis accelerometer sensor was used to capture the subject's movements. The module was placed on the subject's right arm and the signals were transferred to the Biopac machine and stored on a laptop. This setting was used because the movements of the arm capture most of the movements that can induce MA into the signal. However, choosing the optimal setting for the electrodes and the accelerometer sensors is outside the scope of this paper and requires further investigation. The accelerometer signals were bandpass filtered using a Butterworth filter with cutoff frequencies of 0.05 and 2 Hz. A sample of the data that is contaminated with MA is shown in Fig. 4.

The plethysmograph's electrodes were placed on the subject's back between serratus posterior superior and serratus posterior inferior muscles. Similarly, voltage electrodes were placed on the back right beside the current electrodes along the path between them. Fig. 5 shows the placements of the electrodes.

Two experiments were conducted to assess the performance of the proposed ε-tube filtering method. The first experiment was performed to compare the proposed method to the ICA algorithm. The FastICA package, which maximizes the non-Gaussianity, was used in this study. For this experiment, the data were collected from six subjects. The subjects performed a total of 272 maneuvers in 280.6 min (72.0 min of the signals were contaminated by MA). The ICA algorithm requires at least two readings of the IP signal from two different sights. The traditional transthoracic electrode placement was used as the second channel of the IP signal. The second experiment was conducted to compare the proposed method to the RLS and NLMS filtering methods. Thirteen subjects participated in this experiment where a total of 501 maneuvers were performed by the subjects in 589.5 min, where 143.9 min of the signals were contaminated by MA.

TABLE I
Maneuvers That were Performed in the Experiments

Maneuver	Description
1	Raising the arm and holding it up.
2	Dropping the arm after it was held up for 10 second.
3	Raising the arm and dropping it immediately.
4	Imitating the act of drinking a cup of water.
5	Twisting the upper body towards right and back.
6	Twisting the upper body towards left and back.
7	Standing up.
8	Sitting down after 10 seconds.
9	Imitating the act of opening a window.
10	Raising the arm and dropping it continuously.
11	Imitating the act of taking food from a plate and putting it in the mouth continuously.
12	Twisting the upper body towards right and left continuously.
13	While standing, imitating the act of walking (in place).
14	While standing, imitating the act of running (in place).

Subjects were asked to perform several maneuvers to imitate transient and periodic movements in both experiments. The experimented maneuvers are described in Table I. Maneuvers 1–9 are transient movements while maneuvers 10–14 are periodic. Each maneuver was performed roughly three times by each subject, except maneuvers 13 and 14 which were each performed once. All the maneuvers except 7 and 8, 13 and 14 were performed while the subject was sitting on a chair.

After removing the MA's, the respiratory rate is extracted from both the filtered IP and the $EtCO_2$ signals. To do so, the S-transform of the signal is computed and the most dominant frequency component between 0 and 2 Hz is considered to be the respiratory rate at each time t. The S-transform is computed within a sliding window which is 30 s long and a step length of 10 s. The respiratory rate is extracted from 10 s of the signal in the middle of the window. Also, a threshold on the amplitude of the signal is used to detect whether the subject is breathing or not. The extracted respiratory rates from the IP and $EtCO_2$ signals are then compared to assess the performance of the proposed filtering method. No postprocessing has been performed prior to the respiratory rate extraction.

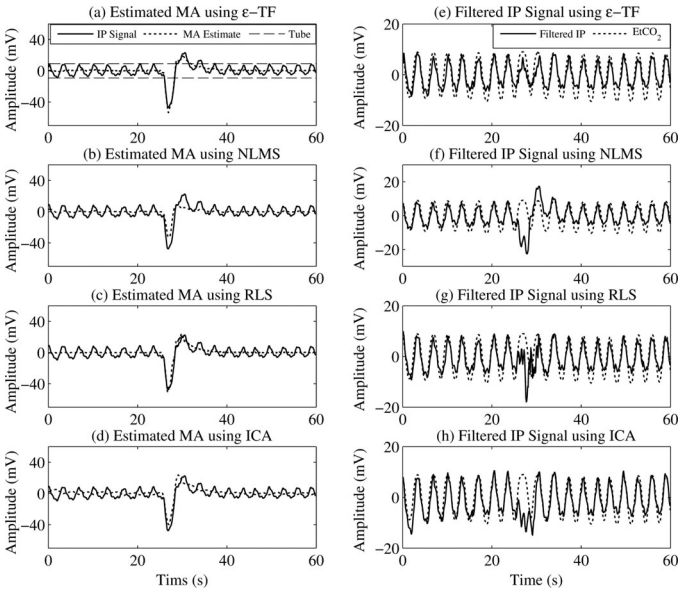

Fig. 6. Motion artifact reduction from an example of maneuver five using the proposed ε-TF method as well as the NLMS, RLS, and ICA methods. (a)–(d) show the contaminated IP signal along with the estimated MA, while (e)–(h) illustrate the signals after MA reduction and the reference $EtCO_2$ signal.

TABLE II
RESULTS OF THE FIRST EXPERIMENT COMPARING ε-TF VERSUS ICA

Method	Corr	Exact	Dev1	Dev3	Mean Err	Max Err
ε-TF	**0.729**	**0.761**	**0.761**	**0.899**	**1.457**	**11.794**
ICA	0.624	0.634	0.634	0.741	4.943	21.066

The numbers in bold indicate the best performance with regards to that performance measure.

TABLE III
RESULTS OF THE SECOND EXPERIMENT COMPARING ε-TF VERSUS RLS AND NLMS

Method	Corr	Exact	Dev1	Dev3	Mean Err	Max Err
ε-TF	**0.680**	**0.690**	**0.690**	**0.855**	**1.894**	**13.558**
NLMS	0.472	0.421	0.538	0.680	4.720	19.759
RLS	0.569	0.509	0.621	0.752	4.626	29.744

The numbers in bold indicate the best performance with regards to that performance measure.

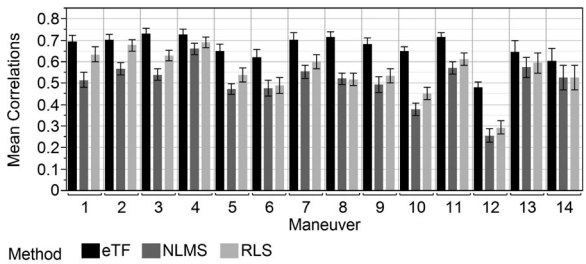

Fig. 7. Comparison between ε-TF, NLMS, and RLS using the mean correlations for different maneuvers. The bars indicate one standard deviation. Notice that ε-TF outperforms NLMS and RLS in all the maneuvers.

VIII. RESULTS AND DISCUSSION

This section presents the results of comparing the respiratory rates extracted from the filtered IP signal and the $EtCO_2$ (reference) signal using two criteria, the error and the correlation, where the error is defined as the amount of discrepancy between the respiratory rates in breaths per minute (BPM). The filter parameters are selected using subject-wise cross validation, i.e., the signals for one of the subjects is used as the test data while the rest of the subjects are used to find the optimal parameters in each fold. The criterion used for selecting the optimal parameters is the mean error. The filter orders for ε-tube were $n_a = 1$ and $n_b = 6$ in all the folds, and $c = 20$ in nine and $c = 10$ in four folds. For the NLMS filter, the selected filter order is 35 in all the folds, the step size is 0.1 in nine folds and 0.05 in the others, and the leakage is 0.93 in six folds and 0.95 for the others. The selected filter orders and forgetting factors for the RLS filters are five and 0.99 in all the folds, respectively. For the ICA algorithm, cross validation selects the tangent hyperbolic AF with $a_1 = 10$ in $\tanh(a_1 u)$ in five folds and the Gaussian AF's with $a_2 = 5$ and $a_2 = 10$ in $u \exp(-a_2 u^2/2)$ for the remaining two folds. The RLS and NLMS filters are chosen as the representatives of the family of adaptive filters since they are the most commonly used filtering methods in different signal processing applications, including MA reduction.

The results of MA reduction using ε-TF, NLMS, RLS, and ICA from a sample of maneuver five are shown in Fig. 6. The amplitude of the filtered IP signal in Fig. 6(b) is within the imposed tube. On the other hand, the NLMS, RLS, and ICA methods, as shown in Figs. 6(f) and (g) do not guarantee that the amplitude of the filtered signal is within the acceptable range of amplitudes for the IP signal. Furthermore, none of the methods except ε-TF are able to successfully recover the respiratory component of the signal. Hence, the proposed method seems to outperform the existing methods. The proposed filter and ICA are compared in Table II using several different performance measures. A similar comparison between the proposed ε-TF, NLMS, and RLS filters is shown in Table III. The first performance measure that is used, *Corr*, is the Pearson correlation coefficient between the filtered IP signal and the $EtCO_2$ signal, which measures how much the morphological features of the two signals agree in the time domain. The error between the extracted respiratory rates is also used to compute several performance measures. The first measure, *Exact*, is the proportion of the times when the extracted respiratory rate from the IP and $EtCO_2$ signals are equal. Moreover, *Dev1* and *Dev3* are the proportions of the times when the average error is less than 1 and 3 BPM, respectively. Finally, *Mean Err* and *Max Err* are the mean and maximum error between the respiratory rates extracted from the filtered IP signal and the $EtCO_2$ signal, respectively.

Figs. 7 and 8 show the comparison between the proposed and the conventional methods for different maneuvers using correlation. The results indicate that the proposed method outperforms the other methods with no exceptions. Moreover, Figs. 9 and 10 show a similar comparison using mean error. Again, the performance of the proposed method is superior to the other methods in all the maneuvers. As a result, we can conclude that the proposed method is more successful in removing the MA compared to ICA, NLMS, and RLS. The statistical significance of the differences are tested using Tukey's honestly significant difference (HSD) for NLMS and RLS and using two-sample *t*-tests for ICA. The Box–Cox transform is successfully applied to the response

TABLE IV
RESULTS OF TWO-SAMPLE t-TESTS OF ε-TF VERSUS ICA, AS WELL AS THE RESULTS OF TUKEY'S HSD TESTS OF ε-TF VERSUS NLMS AND RLS ON MEAN CORRELATIONS ($\alpha = 0.05$)

	Maneuver													
Method	1	2	3	4	5	6	7	8	9	10	11	12	13	14
ICA	✓	✗	✓	✓	✓	✓	✓	✓	✗	✓	✗	✓	✗	✗
RLS	✗	✗	✓	✗	✓	✓	✓	✓	✗	✓	✓	✓	✓	✓
NLMS	✓	✓	✓	✓	✓	✓	✓	✓	✓	✓	✓	✓	✓	✓

The check marks indicate significant differences.

TABLE V
RESULTS OF TWO-SAMPLE t-TEST OF ε-TF VERSUS ICA, AS WELL AS THE RESULTS OF TUKEY'S HSD TESTS OF ε-TF VERSUS NLMS AND RLS ON MEAN ERRORS ($\alpha = 0.05$)

	Maneuver													
Method	1	2	3	4	5	6	7	8	9	10	11	12	13	14
ICA	✓	✓	✓	✗	✓	✓	✓	✓	✗	✓	✓	✓	✗	✗
RLS	✓	✓	✓	✗	✓	✓	✓	✓	✓	✓	✓	✓	✓	✓
NLMS	✓	✓	✓	✗	✓	✓	✓	✓	✓	✓	✓	✓	✓	✓

The check marks indicate significant differences.

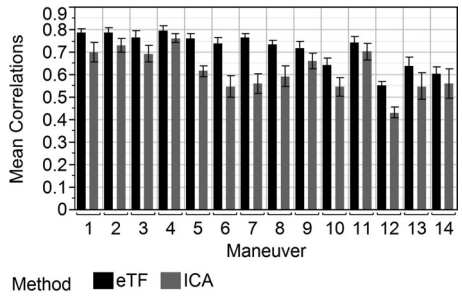

Fig. 8. Comparison between ε-TF and ICA using the mean correlations for different maneuvers. The bars indicate one standard deviation. Notice that ε-TF outperforms the ICA in all the maneuvers.

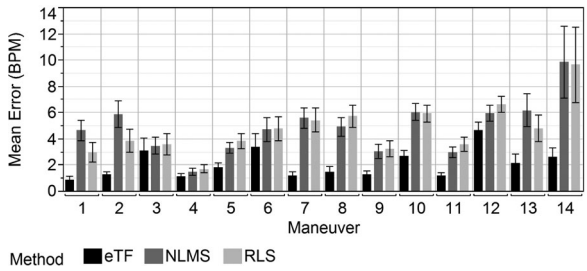

Fig. 9. Comparison between ε-TF, NLMS, and RLS using the mean error for different maneuvers. The bars indicate one standard deviation. Notice that ε-TF outperforms NLMS and RLS in all the maneuvers.

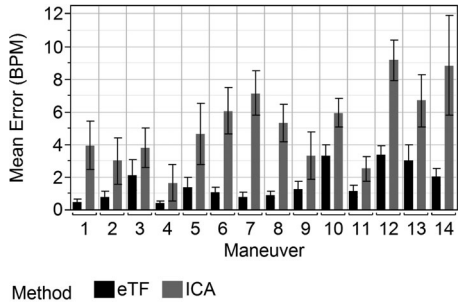

Fig. 10. Comparison between ε-TF and ICA using the mean error for different maneuvers. The bars indicate one standard deviation. Notice that ε-TF outperforms ICA in all the maneuvers.

variables to improve the normality and homogeneity of the variances. The analysis includes *subject* and *replication[subject]* (*replication* nested within *subject*) as random effects, and *filtering method* as a fixed effect. It is performed separately for each maneuver.

The statistical tests indicate that most of the differences in Figs. 7–10 are statistically significant. Tables IV and V show the results of the statistical analysis. The results indicate that 33 of the tests on correlations and 36 of the tests on mean errors out of the total of 42 tests that have been conducted in each case are significant. Similar results are obtained using pair-wise t-tests and Bonferroni's correction, except for the difference between the mean errors of ε-tube and RLS which becomes significant when pair-wise t-test is used. As a result, we can conclude that the proposed method outperforms the existing method and the differences between this method and the existing methods are statistically significant.

All in all, the results indicate that the proposed method is superior compared to ICA, NLMS, and RLS.

IX. CONCLUSION AND FUTURE WORKS

The ε-tube filter proposed in this study is a novel approach for removing high-amplitude MA's from the IP signal with a regular pattern. The only assumption that is made is that the amplitude of the signal of interest does not change rapidly during a short period of time. An ARX model is used to relate the input accelerometer signals to the filter output which is an estimate of the MA. A ε-tube is used to measure the estimation error. This allows for modeling the MA while refraining from modeling the signal of interest. In order to choose the best filter coefficients among those that minimize the estimation error, a regularization term is introduced to maximize the regularity of the output signal. The results show that the ε-tube filter with regularization can effectively reduce the MA in the IP signal. In particular, the proposed method outperforms ICA, NLMS, and RLS in all the maneuvers that were performed in the experiments. The statistical tests indicate that the differences between ε-TF and the conventional methods are statistically significant in most of

the cases. Hence, the proposed method is more successful in removing the MA from the IP signal than ICA, NLMS, and RLS.

One of the future works of this study is to evaluate the performance of ε-tube filter in removing MA's from other physiological signals, such as ECG and PPG. Moreover, the proposed method should be compared to other existing MA reduction methods. The adaptive version of the same filter will also be developed to be used in real-time applications.

APPENDIX

PROOF OF THE SHIFT THEOREM FOR DISCRETE S-TRANSFORM

Consider the Fourier transform of y,

$$y[kT] \overset{\mathcal{F}}{\longleftrightarrow} Y\left(\frac{n}{NT}\right). \tag{58}$$

The Fourier transform of y after a shift of size r is

$$y[(k-r)T] \overset{\mathcal{F}}{\longleftrightarrow} e^{-\frac{j2\pi nr}{N}} Y\left(\frac{n}{NT}\right). \tag{59}$$

Substituting the Fourier transform of $y[(k-r)T]$ into (8) will lead to

$$\begin{aligned}
&\mathcal{S}_{y_{k-r}}\left[pT, \frac{n}{NT}\right] \\
&= \sum_{m=0}^{N-1} Y\left[\frac{m+n}{NT}\right] e^{-\frac{j2\pi(m+n)r}{N}} e^{-\frac{2\pi^2 m^2}{n^2}} e^{\frac{j2\pi mp}{N}} \\
&= e^{-\frac{j2\pi nr}{N}} \sum_{m=0}^{N-1} Y\left[\frac{m+n}{NT}\right] e^{-\frac{2\pi^2 m^2}{n^2}} e^{\frac{j2\pi m(p-r)}{N}} \\
&= e^{-\frac{j2\pi nr}{N}} \mathcal{S}_y\left[(p-r)T, \frac{n}{NT}\right].
\end{aligned} \tag{60}$$

Hence,

$$y[(k-r)T] \overset{\mathcal{S}}{\longleftrightarrow} e^{\frac{-j2\pi nr}{N}} \mathcal{S}_y\left[(p-r)T, \frac{n}{NT}\right]. \tag{61}$$

ACKNOWLEDGMENT

The authors would like to thank BodyMedia Inc. and Dr. A. Belle for their constructive feedbacks. They would also like to thank Dr. K. Gunnerson for his comments and medical advice as the PI for the project IRB. The opinions expressed herein are the personal opinions of the authors and are not to be construed as representing those of the Department of Defense, the Department of the Army, or the U.S. Army.

REFERENCES

[1] J. Ottenbacher, M. Kirst, L. Jatoba, M. Huflejt, U. Grossmann, and W. Stork, "Reliable motion artifact detection for ECG monitoring systems with dry electrodes," in *Proc. IEEE 30th Annu. Int. Conf. Eng. Med. Biol. Soc.*, 2008, pp. 1695–1698.

[2] Y. Liu and M. Pecht, "Reduction of motion artifacts in electrocardiogram monitoring using an optical sensor," *Biomed. Instrum. Technol.*, vol. 45, no. 2, pp. 155–163, 2011.

[3] M. Chawla, "PCA and ICA processing methods for removal of artifacts and noise in electrocardiograms: A survey and comparison," *Appl. Soft Comput.*, vol. 11, no. 2, pp. 2216–2226, 2011.

[4] M. Milanesi, N. Martini, N. Vanello, V. Positano, M. Santarelli, and L. Landini, "Independent component analysis applied to the removal of motion artifacts from electrocardiographic signals," *Med. Biol. Eng. Comput.*, vol. 46, pp. 251–261, 2008.

[5] A. Griffiths, A. Das, B. Fernandes, and P. Gaydecki, "A portable system for acquiring and removing motion artefact from ECG signals," *J. Phys., Conf. Series*, vol. 76, no. 1, 012038, 2007.

[6] M. Milanesi, N. Martini, N. Vanello, V. Positano, M. Santarelli, R. Paradiso, D. De Rossi, and L. Landini, "Multichannel techniques for motion artifacts removal from electrocardiographic signals," in *Proc. IEEE 28th Annu. Int. Conf. Eng. Med. Biol. Soc.*, 2006, pp. 3391–3394.

[7] D. Jeong and S. Kim, "Development of a technique for cancelling motion artifact in ambulatory ECG monitoring system," in *Proc. IEEE 3rd Int. Conf. Convergence Hybrid Inf. Technol.*, 2008, vol. 1, pp. 954–961.

[8] D. Tong, K. Bartels, and K. Honeyager, "Adaptive reduction of motion artifact in the electrocardiogram," in *Proc. IEEE 24th Annu. Int. Conf. Eng. Med. Biol.*, 2002, vol. 2, pp. 1403–1404.

[9] S. Liu, "Motion artifact reduction in electrocardiogram using adaptive filter," *J. Med. Biol. Eng.*, vol. 31, pp. 67–72, 2011.

[10] S. Luo and W. Tompkins, "Experimental study: Brachial motion artifact reduction in the ECG," in *Proc. Comput. Cardiol.*, 1995, pp. 33–36.

[11] M. Raya and L. Sison, "Adaptive noise cancelling of motion artifact in stress ECG signals using accelerometer," in *Proc. IEEE 24th Annu. Int. Conf. Eng. Med. Biol.*, 2002, vol. 2, pp. 1756–1757.

[12] S. Yoon, S. Min, Y. Yun, S. Lee, and M. Lee, "Adaptive motion artifacts reduction using 3-axis accelerometer in e-textile ECG measurement system," *J. Med. Syst.*, vol. 32, no. 2, pp. 101–106, 2008.

[13] M. Ur Rahman, R. Shaik, and D. Reddy, "An efficient noise cancellation technique to remove noise from the ECG signal using normalized signed regressor LMS algorithm," in *Proc. IEEE Int. Conf. Bioinformat. Biomed.*, 2009, pp. 257–260.

[14] L. A. Geddes and L. E. Baker, *Principles of Applied Biomedical Instrumentation*. New York, NY, USA: Wiley, 1968.

[15] A. Pacela, "Impedance pneumography–A survey of instrumentation techniques," *Med. Biol. Eng. Comput.*, vol. 4, pp. 1–15, 1966.

[16] E. Alt, M. Heinz, C. Hirgstetter, H. P. Emslander, S. Daum, and H. Blmer, "Control of pacemaker rate by impedance-based respiratory minute ventilation," *Chest*, vol. 92, no. 2, pp. 247–252, 1987.

[17] L. E. Baker, "Applications of the impedance technique to the respiratory system," *IEEE Eng. Med. Biol. Mag.*, vol. 8, no. 1, pp. 50–52, Mar. 1989.

[18] R. D. Allison, E. L. Holmes, and J. Nyboer, "Volumetric dynamics of respiration as measured by electrical impedance plethysmography," *J. Appl. Physiol.*, vol. 19, no. 1, pp. 166–173, 1964.

[19] D. Warburton, A. R. Stark, and H. W. Taeusch, "Apnea monitor failure in infants with upper airway obstruction," *Pediatrics*, vol. 60, no. 5, pp. 742–744, 1977.

[20] G. Little, R. Ballard, J. Brooks *et al.*, "National institute of health consensus development: Course on infantile apnea and home monitoring, September 1986," *Pediatrics*, vol. 79, pp. 292–299, 1987.

[21] T. M. Baird and M. R. Neuman, "Effect of infant position on breath amplitude measured by transthoracic impedance and strain gauges," *Pediatric Pulmonol.*, vol. 10, no. 1, pp. 52–56, 1991.

[22] S. Luo, V. Afonso, J. Webster, and W. Tompkins, "The electrode system in impedance-based ventilation measurement," *IEEE Trans. Biomed. Eng.*, vol. 39, no. 11, pp. 1130–1141, Nov. 1992.

[23] J. Rosell, K. Cohen, and J. Webster, "Reduction of motion artifacts using a two-frequency impedance plethysmograph and adaptive filtering," *IEEE Trans. Biomed. Eng.*, vol. 42, no. 10, pp. 1044–1048, Oct. 1995.

[24] S. Ansari, K. Ward, and K. Najarian, "ε-tube regression: A new method for motion artifact reduction," in *Proc. IEEE Annu. Int. Conf. Eng. Med. Biol. Soc.*, 2011, pp. 2736–2739.

[25] V. Vapnik, *Statistical Learning Theory* (Series Adaptive and Learning Systems for Signal Processing, Communications, and Control). New York, NY, USA: Wiley, 1998.

[26] R. Stockwell, L. Mansinha, and R. Lowe, "Localization of the complex spectrum: The S transform," *IEEE Trans. Signal Process.*, vol. 44, no. 4, pp. 998–1001, Apr. 1996.

[27] R. Stockwell, "Why use the S-transform," *Pseudo-Differential Operators: Partial Differential Equations and Time-Frequency Analysis* (Fields Inst. Commun. Series), vol. 52. Providence, RI, USA: Amer. Math. Soc., 2007, pp. 279–309.

[28] D. Sarason, *Complex Function Theory*, 2nd ed. Providence, RI, USA: Amer. Math. Soc., 2007.

Sardar Ansari (M'13) received the Bachelor's degree in software engineering from the Department of Electrical and Computer Engineering, University of Tehran, Tehran, Iran, in 2008, and the M.S. degree in computer science from Virginia Commonwealth University (VCU), Richmond, VA, USA, in 2010. He received the M.S. degree in statistics and the Ph.D. degree in computer science from VCU, in December 2013.

He is currently with Virginia Commonwealth University, Richmond, VA, USA. His research interests include signal and image processing, machine learning, and data mining, as well as nonlinear and discrete optimization and queuing theory.

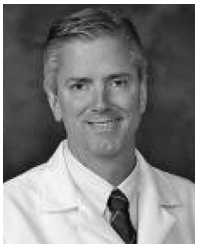

Kevin Ward received the B.S. degree in physiology from Louisiana State University in Baton Rouge and his degree in medicine from Tulane University in New Orleans, LA, USA. He then completed a residency in Emergency Medicine at the University of Pittsburgh, USA.

He is an M.D. and a Professor in the Department of Emergency Medicine, University of Michigan, Ann Arbor, MI, USA. He has published in more than 200 peer-reviewed articles, abstracts, and chapters. His research interests include development of broad platform technologies for the diagnosis, monitoring, and treatment of the critically injured including a focus on combat casualty care. He is an Instrumental Member of the Michigan Critical Injury and Illness Research Center.

Dr. Ward received many awards including the Peter Safar Award in Graduate Research from the University of Pittsburgh, the Society of Academic Emergency Medicines Young Investigator Award, and the U.S. Army's Advanced Technologies Applications in Combat Casualty Care Award. He is also a Prolific Inventor and was awarded the 2010 VCU Billie Martin Innovator of the Year Award.

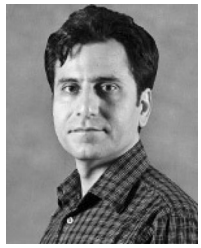

Kayvan Najarian (SM'07) received the B.Sc. degree in electrical engineering from Sharif University, Tehran, Iran, the M.Sc. degree in biomedical engineering from Amirkabir University, Tehran, and the Ph.D. degree in electrical and computer engineering from the University of British Columbia, Vancouver, Canada.

He is an Associate Professor in the Departments of Computational Medicine and Bioinformatics, and Emergency Medicine at the University of Michigan, Ann Arbor, MI, USA. He also serves as the Director of the Michigan Center for Integrative Research in Critical Care's Biosignal-Image and Computational Core program. His research interests include design of signal/image processing and machine learning methods to create computer-assisted clinical decision support systems that improve patient care. Dr. Najarian serves as the Editor-in-Chief of a journal in the field of biomedical engineering as well as the Associate Editor of two journals in the field of biomedical informatics. He is also a Member of many editorial boards and has served as a Guest Editor of special issues for several journals.